ACS Catalysis

Research Article

pubs.acs.org/acscatalysis

Robust Co-catalytic Performance of Nanodiamonds Loaded on WO_3 for the Decomposition of Volatile Organic Compounds under Visible Light

Hyoung−il Kim,[†,§] Hee-na Kim,[†,§] Seunghyun Weon,[†] Gun-hee Moon,[†] Jae-Hong Kim,[‡] and Wonyong Choi*[,†]

[†]Division of Environmental Science and Engineering/Department of Chemical Engineering, Pohang University of Science and Technology (POSTECH), Pohang 37673, Korea

[‡]Department of Chemical and Environmental Engineering, School of Engineering and Applied Science, Yale University, New Haven, Connecticut 06511, United States

Supporting Information

ABSTRACT: Proper co-catalysts (usually noble metals), combined with semiconductor materials, are commonly needed to maximize the efficiency of photocatalysis. Search for cost-effective and practical alternatives for noble-metal co-catalysts is under intense investigation. In this work, nanodiamond (ND), which is a carbon nanomaterial with a unique sp^3(core)/sp^2(shell) structure, was combined with WO_3 (as an alternative co-catalyst for Pt) and applied for the degradation of volatile organic compounds under visible light. NDs-loaded WO_3 showed a highly enhanced photocatalytic activity for the degradation of acetaldehyde (~17 times higher than bare WO_3), which is more efficient than other well-known co-catalysts (Ag, Pd, Au, and CuO) loaded onto WO_3 and comparable to Pt-loaded WO_3. Various surface modifications of ND and photoelectochemical measurements revealed that the graphitic carbon shell (sp^2) on the diamond core (sp^3) plays a crucial role in charge separation and the subsequent interfacial charge transfer. As a result, ND/WO_3 showed much higher production of OH radicals than bare WO_3 under visible light. Since ND has a highly transparent characteristic, the light shielding that is often problematic with other carbon-based co-catalysts was considerably lower with NDs-loaded WO_3. As a result, the photocatalytic activity of NDs/WO_3 was higher than that of WO_3 loaded with other carbon-based co-catalysts (graphene oxide or reduced graphene oxide). A range of spectroscopic and photo(electro)chemical techniques were systematically employed to investigate the properties of NDs-loaded WO_3. ND is proposed as a cost-effective and practical nanomaterial to replace expensive noble-metal co-catalysts.

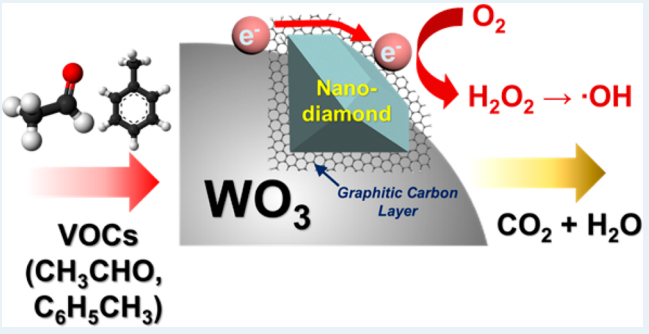

KEYWORDS: *nanodiamond, WO_3, co-catalyst, visible-light photocatalyst, volatile organic compounds, photocatalytic air purification*

INTRODUCTION

Photocatalysis has been recognized as an eco-friendly technology that requires solar light only, without the use of toxic chemicals and additional energy input. It has been actively investigated for environmental remediation such as the degradation of aquatic/air pollutants and the disinfection of microorganisms.[1−3] Volatile organic compounds (VOCs) such as formaldehyde, acetaldehyde, and toluene, are being recognized as major indoor air pollutants and have been frequently employed as model organic compounds for photocatalytic air purification. TiO_2, which is the most popular photocatalyst, has shown superior photocatalytic activities for the degradation of various organic pollutants including VOCs.[4,5] With regard to indoor applications, however, the use of TiO_2, which is a large bandgap semiconductor (~3.2 eV) that absorbs only ultraviolet (UV) photons, is inadequate, because the UV light intensity available in an indoor environment is extremely low and the use of harmful UV lamps is limited in an indoor environment.

Therefore, many studies have focused on developing efficient visible light active photocatalysts that enable the degradation of air pollutants (e.g., VOCs) under indoor light illumination. WO_3 as a potential candidate that can utilize visible light ($E_g \approx$ 2.8 eV) has the valence band (VB) edge located at ~3.0 V_{NHE},[6] providing enough driving force to generate OH radicals as well as to directly decompose various organic pollutants by the direct transfer of VB holes. However, the conduction band (CB) edge potential of WO_3 (~0.4 V vs NHE)[6] is not negative enough to utilize dioxygen as an efficient electron acceptor (i.e., $O_2 + e^- = O_2^{\bullet-}$ ($E^0 = -0.33$ V_{NHE}); $O_2 + H^+ + e^- = HO_2^\bullet$ (E^0

Received: September 23, 2016
Revised: November 2, 2016
Published: November 17, 2016

DOI: 10.1021/acscatal.6b02726
ACS Catal. 2016, 6, 8350−8360

= −0.046 V_{NHE})).[7,8] The inability of O_2 to scavenge the WO_3 CB electrons enhances the charge recombination with a significant decrease of the photocatalytic efficiency.[9,10] Therefore, many recent studies have attempted to achieve an efficient photocatalysis on WO_3 via (1) the loading of novel metals (Cu, Ru, Rh, Pd, Ag, Ir, Pt, Au) and metal oxide (V_2O_5, Cr_2O_3, MnO_2, Fe_2O_3, CoO, NiO, CuO, ZnO, PdO, Ag_2O, RuO_2) as co-catalysts,[11−15] or (2) the hybridization with other semiconductors ($CaFe_2O_4$, $CuBi_2O_4$).[9,16] Among those, so far, the loading of Pt has shown the highest enhancement effect, demonstrating an ∼2-orders-of-magnitude-higher rate for the degradation of gaseous isopropyl alcohol.[13] Pt nanoparticles loaded on WO_3 make the use of O_2 as a CB electron acceptor possible, because the multielectron reduction of O_2 to H_2O_2 (O_2/H_2O_2, E^0 = +0.68 V_{NHE}) or H_2O (O_2/H_2O, E^0 = +1.23 V_{NHE})[17,18] is enabled instead of the single electron reduction ($O_2/O_2^{\bullet -}$), with facilitation of the charge separation and OH radical production.[19] However, the high cost and limited supply of platinum has been always the critical limiting factor in its large-scale application, making the search for inexpensive alternatives to platinum a vital pursuit.

Nanodiamonds (NDs), which were first synthesized in the 1960s,[20] via detonation of carbon-containing explosives under an oxygen-deficient condition, have been utilized in many fields, such as nanoscale sensors,[21] biomedical imaging,[22] drug delivery,[23] and energy applications.[24] Being a relatively inexpensive metal-free nanomaterial (having a cost of a few dollars per gram for ND versus ca. $50 per gram for platinum),[25,26] NDs have a unique structure composed of an sp^3-carbon diamond core and a graphitic (sp^2) carbon outer layer with a diameter of ca. 5 nm, providing many novel characteristics, including chemical and physical inertness, strong fluorescence, tunable surface functionalization, and low toxicity.[27,28] Recently, the photocatalytic activity of TiO_2−ND composite has been studied by a couple of groups. However, most of the studies focused on the role of ND as a support material and an adsorbent for substrates,[29,30] and did not clearly explain the role of ND in its composites.[31]

In this study, we first demonstrated the application of ND as a co-catalyst loaded on WO_3 for VOC degradation under visible light irradiation (λ > 420 nm). ND that is composed of Earth-abundant elemental carbon only exhibited a superior catalytic efficiency for the photocatalytic degradation of VOC, which is comparable to platinum, with regard to its efficiency. The unique structure of ND, consisting of an sp^3 (diamond core) and sp^2 (outer layer) carbon mixture, is responsible for its role as a co-catalyst. In order to study the hybrid effects of NDs and WO_3 for the visible light photocatalytic activity, various photo(electro)chemical measurements and characterizations and the effects of various surface modifications of ND were investigated and discussed.

EXPERIMENTAL SECTION

Preparation of Modified WO_3. *ND-Loaded WO_3.* ND solution (uDiamond Allegro, ca. 5 wt %, ca. 4−6 nm diameter) was purchased and the ND powder that was used for loading onto WO_3 (Aldrich) was obtained by filtering the ND solution and rinsing with 1 M H_2SO_4 and deionized (DI) water several times to remove impurity metals. NDs were modified in various ways to investigate the effects of the modification on the photoactivity. Oxidized NDs (Ox-NDs) were obtained by annealing NDs at 430 °C for 5 h under air in a muffle furnace.[32] Hydrogenated Ox-NDs (H-Ox-NDs) were prepared by annealing Ox-NDs at 800 °C for 2 h under a H_2 flow (150 mL min^{-1}) in a flow furnace.[24] Graphitized NDs (G-NDs) were prepared by annealing NDs at 1200 °C for 2 h under an argon flow (150 mL min^{-1}) in a flow furnace.[33] Acid-purified G-NDs (G(A)-NDs) were prepared by refluxing G-NDs in a 3:1 mixture of HNO_3/H_2SO_4 for 2 h, subsequently washing with DI water several times, and drying at 70 °C for 12 h.

The loading of NDs on the WO_3 surface was accomplished by a simple dehydration condensation between the oxygen-containing functional groups on NDs and the hydroxyl groups on WO_3 surface.[34] To prepare a series of ND-loaded WO_3 with different ND contents (0.5−16 wt %, with respect to the mass of WO_3), ND powder was dispersed in water via ultrasonication, and then a calculated amount of WO_3 was added to the above suspension. The pH of NDs and WO_3 suspension was adjusted, depending on the type of NDs, according to their surface charge (see Figure S1 in the Supporting Information): bare NDs, G-NDs, and G(A)-NDs for pH 2; Ox-NDs for pH 1; H-Ox-ND for pH 4. The suspension was aged for 5 h with vigorous stirring. This suspension then was filtered, washed with DI water several times, and dried overnight at 70 °C.

Graphene Oxide (GO)- or Reduced GO (rGO)-Loaded WO_3. GO was synthesized from graphite (SP-1 grade 200 mesh, Bay Carbon, Inc.) by using a modified Hummers' method[35] and was reduced to reduced GO (rGO) via a simple chemical reduction method, using a hydrazine solution (hydrazine hydrate, Aldrich) at an elevated temperature (90 °C). GO/rGO-loaded WO_3 was prepared using the same procedure as that used for ND-loaded WO_3, except for pH (ca. ≤1). GO/rGO and GO/rGO-loaded WO_3 were characterized by high-resolution X-ray photoelectron spectroscopy (XPS) and field-emission scanning electron microscopy (FE-SEM) analysis (see Figure S2 in the Supporting Information).

Metal (Oxide)-Loaded WO_3. Various metal-loaded WO_3 samples were prepared via a photodeposition method. The followings were used as metal precursors: hydrogen tetrachloroaurate trihydrate ($HAuCl_4 \cdot 3H_2O$, Aldrich, ≥99.9%), chloroplatinic acid hexahydrate ($H_2PtCl_6 \cdot 6H_2O$, Aldrich), palladium chloride ($PdCl_2$, Aldrich, ≥99.999%), silver nitrate ($AgNO_3$, Aldrich, ≥99.0%), and copper chloride ($CuCl_2$, Aldrich, ≥99.999%)). To prepare CuO-loaded WO_3, Cu/WO_3 was annealed at 300 °C for 30 min in air, as reported previously.[12] These metal(oxide) loaded WO_3 were characterized by high-resolution transmission electron microscopy (HR-TEM) and energy-dispersive X-ray spectroscopy (EDS) analysis (see Figure S3 in the Supporting Information). The photocatalyst-coated glass plates with modified WO_3 were prepared by using a doctor blade method, as described previously.[36] The paste of catalyst in ethanol (0.15 g mL^{-1}) was spread on a plate glass slide (40 mm × 20 mm) and then annealed at 200 °C under an argon flow (total loading of photocatalyst on glass plates ≈ 4 mg).

Preparation of Other Visible-Light-Active Photocatalysts for Comparison. To compare the visible light activity of WO_3 with other types of photocatalysts, TaON, Ta_3N_5, C_{60}-TiO_2, C-doped TiO_2, TiO_2−WO_3, CdS, *N*-doped TiO_2 were prepared. This set of photocatalysts were chosen for comparison because they represent various types of visible-light-active materials. Although these materials were prepared using different precursors and methods, the systematic comparison of these photocatalysts with WO_3 would assess whether the choice of WO_3 as a base material in this study is suitable. WO_3 (∼100 nm, Aldrich) and CdS were obtained

DOI: 10.1021/acscatal.6b02726
ACS Catal. 2016, 6, 8350−8360

from Aldrich. TaON and Ta_3N_5 were prepared by nitridation of Ta_2O_5 under NH_3 flow.[37] TiO_2 doped with N (0.4 wt %) was synthesized by a sol−gel method with titanium tetrachloride ($TiCl_4$) and ammonium hydroxide ($NH_3{\cdot}H_2O$) in an aqueous oxalic acid solution (~0.9 M).[38] TiO_2 doped with C (4.4 wt %) was prepared via a hydrothermal method:[39] $Ti(OH)_4$ gel was first prepared by heating an aqueous solution containing titanium tetra-*iso*-propoxide (TTIP, Aldrich, 97%), triethanolamine (TEOA, Aldrich, ≥99%), and oleic acid (Aldrich, ≥99%) in a Teflon-lined autoclave at 100 °C. The gel then was calcined at 250 °C. The N- and C-doped TiO_2 samples were characterized by high-resolution XPS (see Figure S4 in the Supporting Information). C_{60}-TiO_2 was prepared via a simple dehydration method with water-soluble fullerol ($C_{60}(OH)x$).[40] TiO_2−WO_3 composite was synthesized by a sol−gel method with TiO_2 nanoparticles (P25, Degussa) and tungstic acid obtained through the ion-exchange resin from Na_2WO_4 (Aldrich, ≥99%).[41] In order to prepare the various photocatalyst-coated glass plates containing the same amount of catalysts for the acetaldehyde decomposition, 0.2 g of the photocatalyst powder was mixed with ethanol and the entire mixture was casted on a plate glass slide (40 mm × 20 mm) with a spacer (total loading of photocatalyst on glass plates ≈ 200 mg). In this case, the tested photocatalyst mass on the glass plate was higher (200 mg) than the cases of various modified WO_3 samples (4 mg) listed in Table 1. The photocatalyst-coated glass plates were then annealed at 200 °C under an argon flow.

Table 1. Photocatalytic Decomposition of Acetaldehyde with Various Modified WO_3

sample	k_d[a] (× 10^2 min^{-1})	removal[b] (%)	yield of complete oxidation to CO_2[c] (%)
WO_3	0.30	20.8	21.8
Ag (1 wt %)/WO_3	0.06	3.3	6.9
CuO (2 wt %)/WO_3	0.20	11.2	11.5
Pd (0.1 wt %)/WO_3	1.26	52.1	23.1
Au (1 wt %)/WO_3	1.52	59.0	27.2
GO/WO_3	1.59	64.1	41.8
rGO/WO_3	2.89	79.4	39.6
Ox-ND/WO_3	0.12	8.5	14.2
H-Ox-ND/WO_3	3.11	83.1	53.3
G-ND/WO_3	1.56	62.3	38.4
(A)G-ND/WO_3	2.58	77.0	44.4
ND/WO_3	5.16	92.1	65.7
Pt (1 wt %)/WO_3	6.05	99.1	67.9

[a]k_d was estimated by fitting the data (for initial 30 min) from Figures 2 and 3, as well as Figures S11 and S12 in the Supporting Information, through a pseudo-first-order equation. [b]Removal (%) = (Δ-$[CH_3CHO]/[CH_3CHO]_0$) × 100 (after 1 h of reaction). [c]Yield of complete oxidation to CO_2 (%) = ($\Delta[CO_2]/2[CH_3CHO]_0$) × 100 (after 1 h of reaction). All ND-loaded WO_3 samples contained 8 wt % of NDs and (r)GO/WO_3 contained 4 wt % of (r)GO.

Characterization of Photocatalysts. The HR-TEM, energy-dispersive X-ray spectroscopy (EDS), selected-area electron diffraction (SAED), and electron energy loss spectroscopy (EELS) of ND-loaded WO_3 were obtained using a Cs-corrected Model JEM-2200FS microscope (JEOL) (located at the National Institute for Nanomaterials Technology, Pohang, Korea). FE-SEM images of the GO/rGO-loaded WO_3 particles were obtained with a Hitachi Model SU-70 microscope. Diffuse reflectance UV/visible absorption spectra (DRS) of various ND-loaded WO_3 were acquired using a spectrophotometer (Shimadzu, Model UV-2401PC) with an integrating sphere attachment. The X-ray photoelectron spectroscopy (XPS) (VG Scientific, Model ESCALAB250) with monochromatic Al Kα source (1486.8 eV) was employed to analyze various NDs metal(oxide)/WO_3, and GO/rGO. Fourier transform infrared (FT-IR) spectra were obtained using attenuated total reflectance−Fourier transform infrared (ATR-FTIR) (Thermo Scientific Nicolet iS50 FT-IR/ATR). The Raman spectra of various NDs were recorded using a spectrometer (Horiba Jobin-Yvon LabRam Aramis) with 514.5 nm line of an Ar ion laser excitation. The zeta-potentials of various NDs and WO_3 in aqueous suspension were measured as a function of pH using an electrophoretic light scattering spectrophotometer (Model ELS 8000, Otsuka).

Photocatalytic VOC Degradation Measurements. A Pyrex glass reactor (volume, ca. 300 cm^3) with a quartz window (3 cm in radius) was connected to a photoacoustic gas monitor (Model INNOVA 1412i, LumaSense) in a closed-circulation system with a magnetic stirrer to provide the gas circulation (see Figure S5a in the Supporting Information). The reactor that contained a photocatalyst-coated glass plate (40 mm × 20 mm) was placed in a wooden box that housed a 150 W halogen lamp as a light source with a long-pass cutoff filter (λ > 420 nm). The spectral irradiance of the halogen lamp and the transmittance of the long-pass cutoff filter are shown in Figure S5b.

The photocatalyst film was preirradiated by UV light for 1 h under flowing pure air to degrade organic impurities on photocatalyst surface until no signal of CO_2 from organic impurity degradation was observed. After the surface cleaning, the reactor was purged with high-purity air (20% O_2, 80% N_2). For the photocatalytic activity test, a specific concentration of acetaldehyde or toluene gas stream was introduced into the reactor from the standard gas (1000 ppmv acetaldehyde, 300 ppmv toluene in Ar) and circulated for 30 min. The concentration of acetaldehyde and toluene used in all experiments was adjusted by diluting with carrier gases (N_2 (99.9999%), O_2 (99.9999%)) which was passed through the water bottle to keep the water vapor concentration at ca. 70% relative humidity. The initial concentration of acetaldehyde and toluene was typically 100 ppmv (except for the multicycle test (30 ppmv)) and 20 ppmv, respectively. After 30 min equilibration of acetaldehyde adsorption, the photocatalyst sample started to be irradiated by visible light. The degradation of acetaldehyde (or toluene) and the concurrent generation of CO_2 were monitored in real time by a photoacoustic gas monitor and were recorded once a minute. The incident visible light flux of the halogen lamp was measured to be ca. 18 mW cm^{-2}, using a thermopile head (Newport, Model 818P-001-12) connected to an optical power meter (Newport, Model 1918-R).

Photoelectrochemical and Photochemical Measurements. Photoelectrochemical (PEC) measurements were carried out in a conventional three-electrode system connected to a computer-controlled potentiostat (Gamry, Reference 600). The PEC reactor contained the photoanode, a coiled Pt wire, and a Ag/AgCl/KCl (sat) electrode as a working, a counter and a reference electrode, respectively, which were immersed in an aqueous electrolyte of 0.1 M $HClO_4$. The photoanodes were prepared on fluorine-doped tin oxide (FTO) glass slides (Pilkington, TEC8) by a method similar to the preparation of the photocatalyst-coated glass plates for VOC degradation tests.

DOI: 10.1021/acscatal.6b02726
ACS Catal. 2016, 6, 8350−8360

The prepared photoanodes had an average active area of ca. 1 cm^2. All PEC measurements were carried out under photoirradiation with a 150 W xenon arc lamp (Oriel) connected to a cutoff filter (λ > 320 nm). The incident light intensities were measured to be ~300 mW cm^{-2}.

The photocurrent was also collected from the suspension of the photocatalyst without using the catalyst-coated electrode.[42] In this case, the photocurrent was collected on an inert electrode (Pt) through electron shuttles (using a reversible redox couple of Fe^{3+}/Fe^{2+}) in the aqueous suspension of photocatalysts under illumination ([catalyst] = 1 g L^{-1}, [$LiClO_4$] = 0.1 M, [Fe^{3+}] = 0.1 mM, pH_i 1.8, λ > 320 nm). The electrolyte solution was continuously purged with N_2 flow during the measurement, and the working electrode (a Pt wire) was biased with an applied potential of +0.9 V (vs Ag/AgCl).

Electrochemical oxygen reduction tests were conducted with a glassy carbon electrode upon which catalyst was deposited. Catalyst-deposited glassy carbon electrodes were obtained by loading a mixture solution containing catalysts and the binder.[43] WO_3 or ND/WO_3 (10 mg) were mixed with a 60 μL of Nafion resin (Alfa Aesar, 5 wt %) as a binder and 800 μL of 2-propanol (Aldrich). The mixture solution (5 μL) then was deposited on a glassy carbon electrode (eDAQ), followed by drying at room temperature and then in a convection oven (105 °C).

The H_2O_2 generation experiments were carried out by irradiating visible light (150 W xenon arc lamp) to the aqueous suspension of photocatalysts with the experimental conditions of [catalyst] = 1 g L^{-1}, pH_i 2 (adjusted by $HClO_4$), O_2-purged, and λ > 420 nm (250 mW cm^{-2}). The concentration of H_2O_2 was determined by the DPD (*N*,*N*-diethyl-1,4-phenylenediamine) colorimetric method,[44] using a UV/visible spectrophotometer (λ_{max} = 551 nm, ε = 21 000 M^{-1} cm^{-1}).

The generation of hydroxyl radical on the illuminated photocatalyst was confirmed by a coumarin method, which monitors the photocatalytic production of 7-hydroxycoumarin (7-HC) through the reaction of hydroxyl radical with coumarin.[45] Coumarin (6.8 mM) was added to the photocatalyst suspension containing 1 g L^{-1} of WO_3 or ND (8 wt %)/WO_3, which was subsequently irradiated under a 150 W xenon arc lamp (Oriel) connected to a cutoff filter (λ > 420 nm). The incident light intensities were measured to be ~250 mW cm^{-2}. Aliquots of the suspension were withdrawn from the reactor every 20 min during the irradiation period and filtered through a 0.45 μm PTFE syringe filter (PALL) to remove catalyst particles. The concentration of 7-HC was estimated spectrofluorometrically by monitoring the emission intensity at 455 nm under the excitation of 332 nm, using a spectrofluorometer (Shimadzu, Model RF-5301).

RESULTS AND DISCUSSION

Characterization of ND-Loaded WO_3. The structural properties of ND-loaded WO_3 (ND(8 wt %)/WO_3) were characterized by HR-TEM, SAED, and EELS analysis. Figures 1a and 1b show the HR-TEM images of ND(8 wt %)/WO_3. The surface of ND(8 wt %)/WO_3 was partially covered by several ND nanoparticles while the surface of WO_3 was considerably covered by ND nanoparticle aggregates on ND (16 wt %)/WO_3 (see Figure S6 in the Supporting Information). The ND nanoparticles (blue circles) on WO_3 are ~2−10 nm in size and had a graphitic carbon layer (≤1 nm) on their surface region.[28,46] The lattice spacing in ND particles is ~2.05 Å, which corresponds to the (111) crystallographic plane of diamond (see Figures 1c and 1d).[46,47] The EELS elemental mapping analysis (Figures 1e−h) was carried out to confirm the presence of NDs and WO_3. The clear mapping images of carbon, tungsten, and oxygen elements revealed that the small nanoparticles on WO_3 are truly NDs.

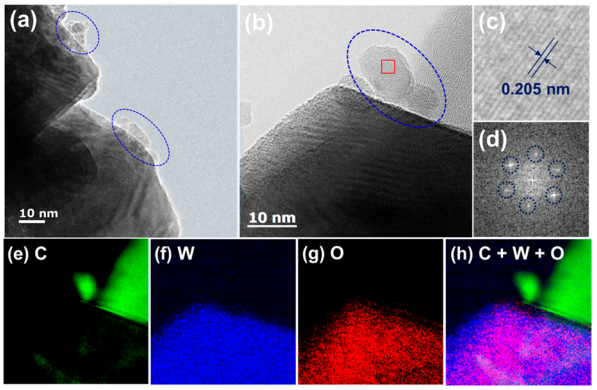

Figure 1. (a, b) HR-TEM images of ND(8 wt %)/WO_3. (c) Magnified HR-TEM image from selected area (red square in panel (b)). (d) SAED pattern of the region depicted in panel (c). (e−h) EELS elemental maps of C (panel (e)), W (panel (f)), O (panel (g)), and C + W + O (panel (h)) in ND(8 wt %)/WO_3. Inset in panel (a) shows a magnified HR-TEM image of a ND nanoparticle in ND (8 wt %)/WO_3. The crystallographic (111) diamond interplanar spacing (panel (c)) and diffraction dots of the reciprocal space (panel (d)) indicate the diamond crystalline structure.

Figure S7a in the Supporting Information showed the FT-IR spectra of bare WO_3 and ND(8 wt %)-loaded WO_3. A broad peak centered at 1620 cm^{-1} increased after ND loading, which corresponds to the vibration of C=C (or O−H) on which ND has a strong intensity, derived from the surface graphitic carbon layer (see inset in Figure S7a).[30,48] ND loading marginally changed the absorption spectrum of WO_3 (see Figure S7b). The absorption edge was not shifted while the slight absorption shoulder was observed in the range from 450 nm to 700 nm in DRS. The insignificant change of the absorption spectrum is attributed to the highly transparent characteristic of diamond,[49] unlike other carbon nanomaterials (e.g., GO, rGO, and carbon nanotubes (CNTs)). The results from HR-TEM, SAED, EELS mapping, FT-IR, and DRS analysis clearly indicate that ND particles are successfully loaded on WO_3 with partial surface coverage.

Photocatalytic VOC Degradation on ND/WO_3. Various visible-light-active photocatalysts, including TaON, Ta_3N_5, C_{60}-TiO_2, C-doped TiO_2, TiO_2−WO_3, CdS, *N*-doped TiO_2, and WO_3, were tested for the degradation of acetaldehyde under visible-light illumination (halogen lamp, λ > 420 nm, see Figure S8 in the Supporting Information) and WO_3 exhibited the highest activity. Therefore, WO_3 was chosen as the base photocatalyst for NDs loading in this study. To be compared with NDs, several co-catalysts, known as effective co-catalysts for the photocatalytic degradation of organic compounds when they are combined with WO_3,[11−15] were also compared. Figure 2a shows the amount of acetaldehyde degradation and the concurrent CO_2 production on illuminated WO_3 in the presence of various metal(oxide) as co-catalysts. Ag and CuO decreased the activities in contrast with the previous studies (possibly caused by different preparation methods)[12,15] but Pt, Pd, and Au loading considerably enhanced the activities, compared to that of bare WO_3 under visible-light illumination (λ > 420 nm). Table 1 summarizes the acetaldehyde degradation rate constants (k_d), removal efficiency (%), and

DOI: 10.1021/acscatal.6b02726
ACS Catal. 2016, 6, 8350−8360

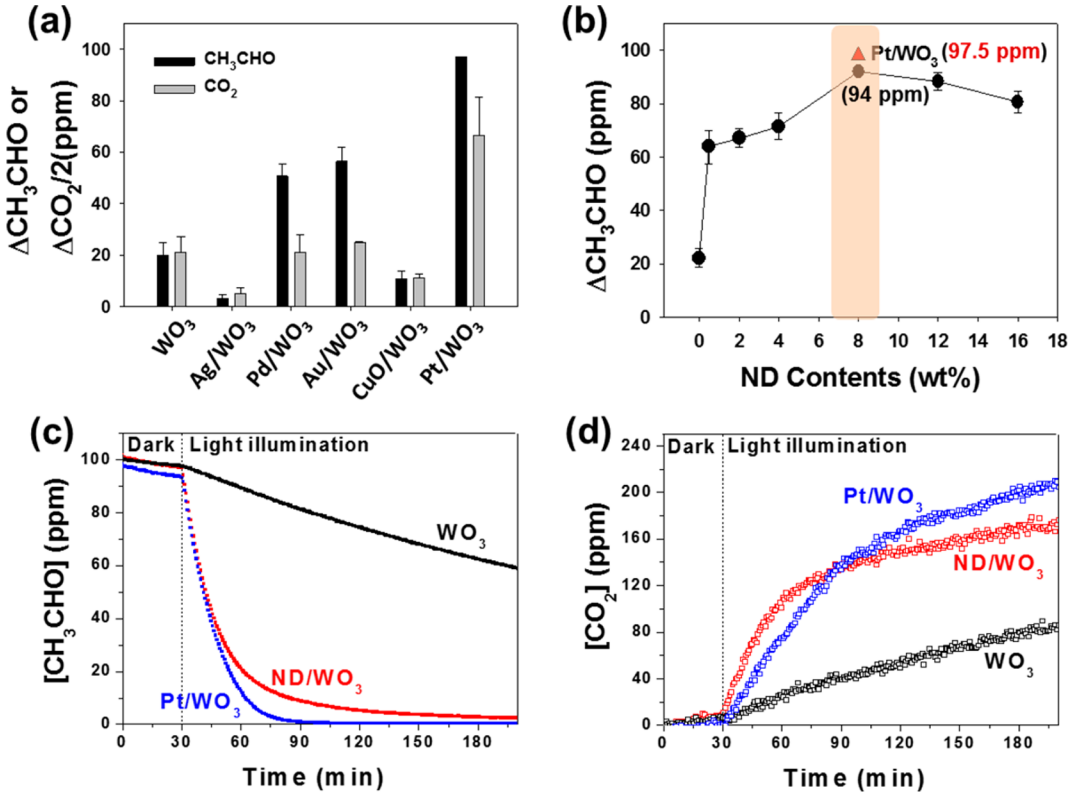

Figure 2. (a) Photocatalytic degradation of acetaldehyde (CH_3CHO) and the concurrent production of carbon dioxide (CO_2) on WO_3 loaded with various co-catalysts (Ag (1 wt %), Pd (0.1 wt %), Au (1 wt %), CuO (2 wt %), and Pt (1 wt %)). (b) Photocatalytic degradation of CH_3CHO on ND-loaded WO_3, as a function of ND loading (wt %). (c, d) Time-dependent profiles of the photocatalytic degradation of CH_3CHO (panel (c)) and the concurrent production of CO_2 on bare WO_3, ND(8 wt %)/WO_3, and Pt(1 wt %)/WO_3 (panel (d)). ΔCH_3CHO and ΔCO_2 represent the amount of removed CH_3CHO and produced CO_2 after 1 h of illumination, respectively. The solid red triangle in panel (b) denotes the amount of CH_3CHO removal on Pt(1 wt %)/WO_3 after 1 h of illumination. $[CH_3CHO]_0$ = 100 ppmv, under visible-light illumination (λ > 420 nm).

conversion to CO_2 (%) for various modified WO_3 photocatalysts. The increased activities on Pt-, Pd-, and Au-loaded WO_3 are likely due to the interfacial electron transfer from CB of WO_3 to co-catalysts.[13] Among them, Pt exhibited the highest activity for both the removal of acetaldehyde and the production of CO_2. The platinum effect for the photocatalytic degradation of acetaldehyde was optimal at 1% Pt loading (see Figure S9 in the Supporting Information).

The loading of NDs as a new carbon-based co-catalyst significantly enhanced the photocatalytic activity of WO_3 to a level that can be comparable to that of Pt-loaded WO_3 (see Table 1). Generally, pure diamond with a bandgap of ca. 5.4 eV (ref 50) as an insulator cannot facilitate charge transfer like other co-catalysts (e.g., Pt, Pd, graphene), which can withdraw electrons from the CB of WO_3 and subsequently transfer them to substrates to initiate redox reactions. However, the NDs contain not only the diamond structure (in core) but also the graphitic carbon layer on their surface region (see Figure 1a),[28,32] enabling NDs to withdraw electrons and transfer them to the reactants. As shown in Figure 2b, the loading of ND drastically increased the activity of acetaldehyde degradation and 8 wt % loading showed an optimal effect: ND(8 wt %)/WO_3 was comparable to Pt(1 wt %)/WO_3. The NDs effect was slightly reduced when further increasing the ND content above 8%, which could be ascribed to the light shielding by the agglomerated excess NDs formed on the surface of WO_3, which was similarly observed with other carbon-based co-catalysts (CNT and graphene) on metal oxide.[51−53] Figures 2c and 2d showed the time profiles of acetaldehyde degradation and the accompanying production of CO_2 on WO_3, ND(8 wt %)/WO_3, and Pt(1 wt %)/WO_3 under visible-light irradiation. Unlike bare WO_3, ND- and Pt-loaded WO_3 degraded acetaldehyde almost completely with a near-stoichiometric conversion to CO_2 ($CH_3CHO + {}^5/_2O_2 \rightarrow 2CO_2 + 2H_2O$) within 150 min of visible-light illumination. It is noted that the acetaldehyde removal profiles are not exactly correlated with the concurrent CO_2 generation profiles for ND/WO_3 and Pt/WO_3, which implies that the intermediate generation and the mechanism might be different, depending on the type of photocatalysts. However, the overall conversion of acetaldehyde to CO_2 is generally consistent with the acetaldehyde removal trend. Toluene, which is another major indoor air pollutant, was also tested as a model VOC (see Figure S10 in the Supporting Information). While toluene was hardly decomposed by WO_3 (<10%) under visible-light illumination (λ > 420 nm), the loading of NDs (8 wt %) on WO_3 significantly enhanced the degradation (~35%). The toluene removal rate was decelerated over the course of the reaction, which can be ascribed by the accumulation of degradation intermediates on the photocatalyst surface.[54] On the other hand, CO_2 (as a final product) was continuously produced without showing a noticeable deceleration, indicating that, as both toluene and intermediates were simultaneously decomposed to form CO_2, the degradation efficiency from photocatalysts remains steady over time.

To further confirm the superiority of NDs as a co-catalyst, WO_3 combined with GO or rGO, known as efficient carbon-based co-catalysts, were also tested for the photocatalytic decomposition of acetaldehyde. Figure S11 in the Supporting

DOI: 10.1021/acscatal.6b02726
ACS Catal. 2016, 6, 8350−8360

Information showed the photocatalytic degradation of acetaldehyde and the accompanying production of CO_2 on GO/WO_3 and rGO/WO_3 with varying contents (0.5−8 wt %). Similar to the case of NDs, the addition of GO (or rGO) onto WO_3 enhanced the photocatalytic degradation, showing a maximum efficiency at a GO loading of ∼4 wt %, indicating that GO and rGO also act as a co-catalyst for the acetaldehyde degradation. rGO that has a higher electronic conductivity than GO showed higher activity. Although both GO- and rGO-loaded WO_3 exhibited the enhanced photocatalytic activity, ND/WO_3 (k_d = 0.052 min^{-1}) displayed even greater activities than GO/WO_3 (k_d = 0.016 min^{-1}) and rGO/WO_3 (k_d = 0.029 min^{-1}). A greater improvement in the acetaldehyde degradation on ND/WO_3, compared to GO/WO_3 and rGO/WO_3, might be ascribed to the different interfacial characteristics between ND/WO_3 and (GO or rGO)$/WO_3$. As demonstrated in a previous study,[34] the relative geometry of the rGO/semiconductor nanoparticle composite structure sensitively influences the photocatalytic reactivity. In addition, GO and rGO sheets absorb and shield a significant fraction of incident light,[55] whereas NDs with a smaller size (∼10 nm) and a relatively small portion of sp^2 carbon (<1 nm thickness of the surface shell) can minimize the light shielding problem.

Effect for Various Modifications of ND for Photocatalytic VOC Degradation. Various modified NDs-loaded WO_3 samples were tested to investigate the effects of ND surface property change on the photocatalytic activity. Figure 3 shows the time profiles of acetaldehyde degradation and the accompanying production of CO_2 on modified ND/WO_3. After the heat treatment (at 420 °C) under air, the photocatalytic activity of oxidized-NDs (Ox-NDs)$/WO_3$ was dramatically reduced and even lower than that of bare WO_3. This might be ascribed to the removal of the surface graphitic carbon layer during the heat treatment (in oxidative environment), which makes the surface of ND nonconducting. However, the photocatalytic activity of Ox-ND could be significantly recovered after hydrogen treatment (H-Ox-ND), which implies that the surface conductivity of ND can be significantly increased by the hydrogen treatment.[56,57] These results indicate that the surface conductivity of ND loaded on WO_3 plays a critical role in the overall photocatalysis.

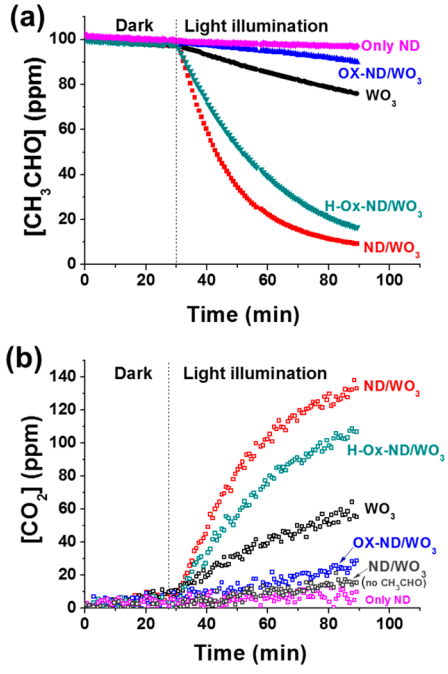

Figure 3. Time-dependent profiles of (a) photocatalytic degradation of acetaldehyde (CH_3CHO) and (b) the concurrent production of carbon dioxide (CO_2) on modified ND/WO_3, bare WO_3, and bare ND. All ND-loaded WO_3 samples contained 8 wt % ND. $[CH_3CHO]_0$ = 100 ppmv, under visible-light illumination (λ > 420 nm). Dark-gray squares (ND/WO_3 (no CH_3CHO)) in panel (b) represent CO_2 generation in the blank control experiment without acetaldehyde.

The surface structure change of NDs was monitored by FT-IR, Raman, X-ray photoelectron spectroscopy (XPS), and HR-TEM for bare NDs, Ox-NDs, and H-Ox-NDs (see Figure 4). HR-TEM images showed that the graphitic carbon layers on the surface of bare ND were indeed removed by the thermal oxidation treatment under air and the crystalline diamond structure was exposed (see Figures 4a and 4b). FT-IR spectra of bare NDs, Ox-NDs, and H-Ox-NDs also showed clear differences (see Figure 4c). The main IR peaks of bare ND include C═C skeletal or O−H bending (1620−1660 cm^{-1}), C═O stretching (1728−1757 cm^{-1}), and O−H stretching (3280−3675 cm^{-1}) vibrations.[32,58,59] After oxidation, the C═O stretch vibration was upshifted to 1790 cm^{-1} and became much stronger, which is attributed to the generation of more oxygen-containing surface functionalities.[32] The hydrogenation treatment on Ox-NDs resulted in the complete disappearance of C═O and the appearance of $C-H_x$ (2800−3000 cm^{-1})[60] stretch vibrations, which indicate that the surface oxygen functional groups of Ox-NDs were mostly transformed to H-termination groups after the hydrogen treatment.

A similar observation was also confirmed by the Raman spectra (see Figure 4d). The Raman spectrum of bare NDs contained three major peaks, consisting of the diamond peak at ∼1323 cm^{-1}, which was downshifted from that of single-crystal diamond (at ∼1332 cm^{-1}),[61,62] the disorder-induced double-resonance D-band at ∼1410 cm^{-1}, and the graphite G-band at ∼1587 cm^{-1}.[63] The thermal oxidation treatment substantially enhanced the diamond signal. The ratio between the diamond (at ∼1323 cm^{-1}) and the G-band (at ∼1587 cm^{-1}) intensities was also significantly enhanced after thermal oxidation treatment, suggesting that the surface nondiamond layer was removed and the diamond phase was exposed during the oxidation treatment. The following hydrogen treatment restored the ratio between the diamond and G-band peaks.[64] The XPS analysis of O 1s band also revealed that the surface oxygen-containing groups were enhanced after the oxidation treatment and reduced after further hydrogen treatment (see Figure 4e). The XPS oxygen content analysis of various ND and GO samples shows that the treatment conditions (reductive or oxidative) critically affect the surface oxygen composition (see Table S1 in the Supporting Information).

Since the presence of the graphitic carbon layer seems to be critical for the photocatalytic activity of ND/WO_3, the effect of the surface graphitic carbon layer on ND was further investigated by increasing the graphitic layer thickness through a high-temperature graphitization at 1200 °C for 2 h under an argon flow (see Figure S12 in the Supporting Information). However, after the high-temperature graphitization, the photocatalytic activity of graphitized-ND (G-ND)$/WO_3$ was reduced from that of ND/WO_3. Possible explanations are (i) the aggregation of ND particles due to the high-temperature treatment, which can reduce the active surface area, (ii) the increase of the light shielding effect by the increase of the sp^2-

DOI: 10.1021/acscatal.6b02726
ACS Catal. 2016, 6, 8350−8360

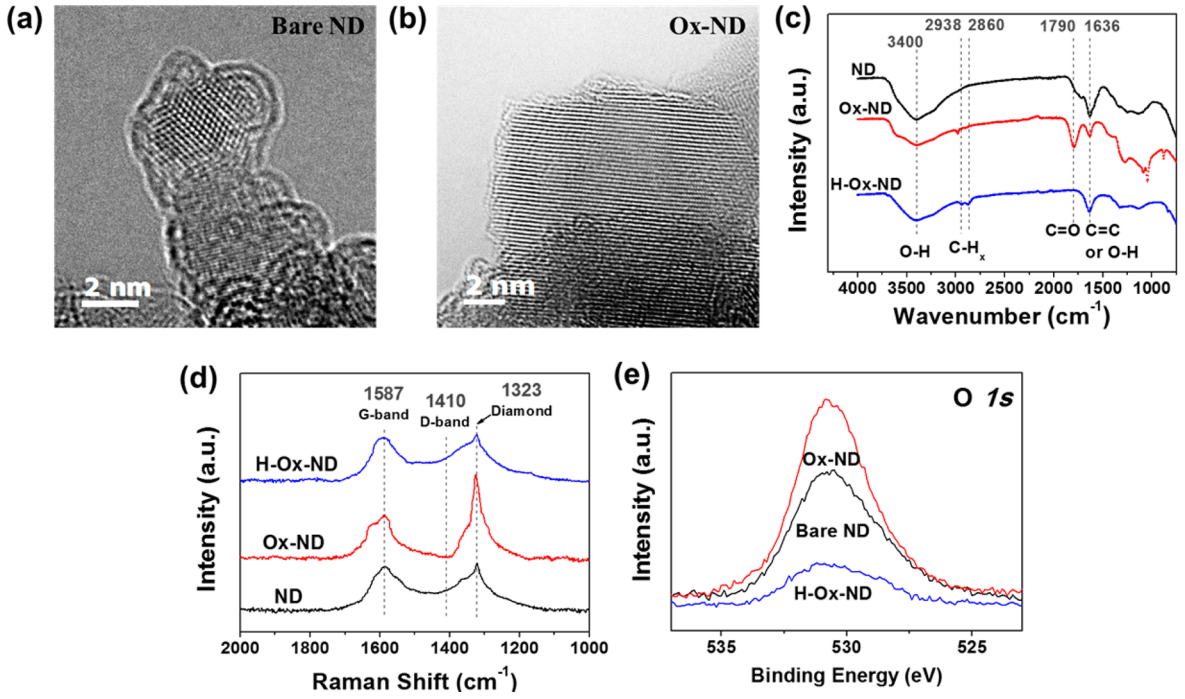

Figure 4. HR-TEM images of (a) bare ND and (b) Ox-ND. (c) FT-IR (between 4000 and 750 cm^{-1}), (d) Raman, and (e) high-resolution XPS spectral band (O 1s) of bare ND, Ox-ND, and H-Ox-ND.

carbon layer, and (iii) the surface property change (e.g., more hydrophobic and less oxygen-containing surface functionality), which leads to a weaker connection between WO_3 and NDs. The HR-TEM image in Figure S12c showed that an agglomerate of G-NDs with an onion-like structure contains a reduced diamond core surrounded by thicker graphitic carbon layers (ca. 2 nm). To improve the dispersibility and obtain a stronger connection with WO_3, the surface of G-NDs was treated with a strong acid oxidant (3:1 of HNO_3/H_2SO_4) to provide oxygen containing functionalities. The photocatalytic activity of G-ND/WO_3 could be enhanced by an acid treatment (3:1 of HNO_3/H_2SO_4) because the acid-treated G-NDs (G(A)-NDs) that contain higher oxygen functionalities on its surface can improve the dispersibility and have a stronger connection with WO_3 (see Figure S12a). The results of the various modifications of NDs indicate that the surface graphitic carbon layer on NDs indeed plays a crucial role to withdraw/transfer electrons but the thicker graphitic carbon layers have adverse effects for the contrary photocatalytic activity.

Interfacial Electron Transfer, Charge Separation, and OH Radical Generation on ND/WO_3. The photoelectrochemical (PEC) properties of ND(8 wt %)/WO_3 were investigated using two types of measurements: slurry-type and electrode-type. For the slurry-type photocurrent measurement, the photogenerated electrons were collected in an aqueous catalyst suspension through the Fe^{3+}/Fe^{2+} redox shuttle under photoirradiation (λ > 320 nm, see Figure 5a). The photocurrent generated in the suspension of WO_3 was significantly improved after loading ND or Pt, while, in contrast, loading Ox-ND on WO_3 reduced the photocurrent generation. This trend is consistent with their photocatalytic activities. Under illumination, photogenerated electrons transfer from WO_3 CB to ND (or Pt) and then subsequently reduce Fe^{3+} on ND/WO_3 (or Pt/WO_3), which is then reoxidized on the collector electrode to generate photocurrent ($Fe^{2+} \rightarrow Fe^{3+} + e^-$). The fact that the photocurrent generation was enhanced with ND loading and reduced with Ox-ND loading confirms that the CB electrons are transferred to the ND phase (in the presence of conducting surface graphitic carbon layer on ND) to retard the charge recombination and facilitate the interfacial charge transfer. The low photocatalytic activity of Ox-ND/WO_3 is ascribed to the absence of the surface graphitic layer. On the other hand, the photocurrent measured with the photocatalyst-coated electrode showed depressed photocurrents on all WO_3 electrodes modified with Pt, ND, and Ox-ND, compared to bare WO_3 (see Figure 5b). Unlike the slurry-type photocurrent measurement, the electrons on bare and modified WO_3 electrodes should migrate through a series of particle boundaries (within the coated WO_3 film) to reach the FTO to be collected as photocurrent. Therefore, Pt and ND nanoparticles on WO_3 that serve as an electron reservoir should trap electrons during their migration through the particle grain boundaries, reducing the photocurrent collection at the FTO, similar to previous published reports.[48,65] The lowest photocurrent of Ox-ND/WO_3 after being deposited on the FTO reconfirms that Ox-ND (with the absence of the surface graphitic layer) significantly retarded electron transfer during the photocurrent collection. Although Ox-ND is largely an insulator that cannot attract electrons, the oxidized functional groups on the ND surface seems to react with and consume electrons, to reduce the photocurrent. It might be also possible that the oxidized functional groups serve as an external recombination center of charge carriers.

The ND nanoparticles coated with the graphitic layer (as shown in the inset of Figure 1a) seem to behave similar to Pt co-catalysts. The electrocatalytic role of ND covered with the graphitic layer was confirmed by comparing the electrochemical reduction of O_2 on WO_3 and ND/WO_3 electrodes. As shown in Figure 5c, the onset potential of dioxygen reduction on WO_3 was positively shifted by ca. 100 mV upon loading ND, which indicates that the ND loading significantly reduced the oxygen reduction overpotential and facilitated efficient oxygen

DOI: 10.1021/acscatal.6b02726
ACS Catal. 2016, 6, 8350−8360

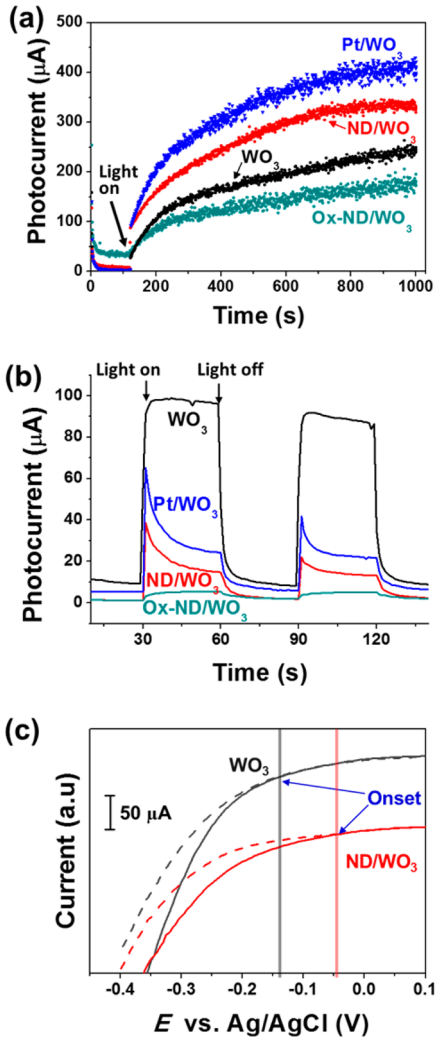

Figure 5. (a) Time-dependent profiles of Fe^{3+}-mediated photocurrent collected on a Pt electrode in the catalyst suspension of WO_3, Pt(1 wt %)/WO_3, Ox-ND(8 wt %)/WO_3, and ND(8 wt %)/WO_3. The experimental conditions were [catalyst] = 1 g L^{-1}, [Fe^{3+}] = 0.1 mM, [$LiClO_4$] = 0.1 M, pH_i 1.8 (by $HClO_4$), Pt electrode held at +0.9 V (vs Ag/AgCl), N_2-purging, and λ > 320 nm. (b) Photocurrent response on the electrode of WO_3, Pt(1 wt %)/WO_3, Ox-ND(8 wt %)/WO_3, and ND(8 wt %)/WO_3 under the repeated light on/off irradiation. [$HClO_4$] = 0.1 M, N_2 purging, and λ > 320 nm. Note that the irradiation of λ > 320 nm (not λ > 420 nm) was employed in panels (a) and (b), to obtain higher photocurrents and higher signal-to-noise ratios, because they were very low under λ > 420 nm. (c) Linear sweep voltammograms of WO_3 and ND(8 wt %)/WO_3 under N_2 or O_2 environment, [$HClO_4$] = 0.1 M; the dashed line represents the condition of N_2 pursing and the solid line represents the condition of O_2 pursing. The onset potentials of the O_2 reduction on the WO_3 and ND/WO_3 electrode are indicated.

reduction.[66] This is similarly compared with the co-catalytic role of Pt for the multielectron reduction of O_2, which should be related with the role of surface graphitic layer on ND in facilitating the multielectron transfer. The Pt-like behavior of reduced graphene oxide has been demonstrated for TiO_2 photocatalysis.[58] A similar behavior of the surface graphitic layer on ND is expected.

The Pt-like catalytic nature of ND with the graphitic layer was also confirmed in the photocatalytic production of H_2O_2 through O_2 reduction in the aqueous suspension of ND/WO_3.

Figure 6 compares the time profiles of the photocatalytic production and decomposition of H_2O_2 between bare WO_3 and

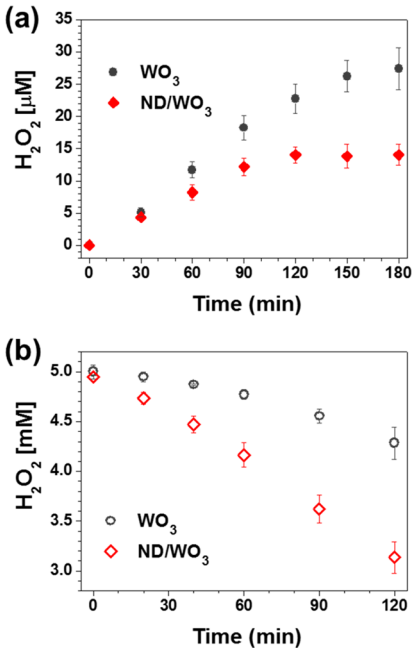

Figure 6. Time profiles of (a) photocatalytic production and (b) photocatalytic decomposition of H_2O_2 on bare WO_3 and ND(8 wt %)/WO_3. The experimental conditions were [catalyst] = 1 g L^{-1}, pH_i 2, O_2-purged, and λ > 420 nm, $[H_2O_2]_0$ = 5 mM for panel (b).

ND/WO_3 under visible-light illumination (λ > 420 nm). The production of H_2O_2 on ND/WO_3 was lower than that on bare WO_3, despite the fact that ND/WO_3 has a lower overpotential of O_2 reduction than bare WO_3 (as shown in Figure 5c). However, note that the overall production of H_2O_2 is determined by not only the forward reaction of O_2 reduction but also the backward decomposition of *in situ*-generated H_2O_2.[48] The decomposition of H_2O_2 was much faster on ND/WO_3 than bare WO_3 (Figure 6b). The fact that the rate of H_2O_2 production in Figure 6a shows little difference between bare WO_3 and ND/WO_3 in the initial period (<30 min) but was markedly decelerated with time supports the belief that the lower production of H_2O_2 on ND/WO_3 should be ascribed to the rapid decomposition of *in situ*-generated H_2O_2. Such behavior of ND/WO_3 is very similar to that of Pt/TiO_2 for the photocatalytic production of H_2O_2.[48] Although platinum is an excellent co-catalyst for many photocatalytic conversions, Pt/TiO_2 shows very poor activity for the photocatalytic production of H_2O_2, because platinum catalyzes the decomposition of H_2O_2 as soon as it is generated.

The strongest oxidant generated in semiconductor photocatalysis is the hydroxyl radical (•OH), but the hydroxyl radical generation is not favored on bare WO_3, because the lower-lying CB potential (~0.4 V vs NHE) does not make the scavenging of CB electrons by O_2 possible.[6] However, it can be strongly enhanced on Pt/WO_3, because platinum allows the multielectron reduction of O_2.[13,19] If ND loaded on WO_3 plays a role similar to that of platinum (as demonstrated in the above), it is expected that the loading of ND on WO_3 also enhances the production of OH radicals under visible-light irradiation. To test this hypothesis, the photocatalytic generation of OH radicals was evaluated indirectly by monitoring the production

DOI: 10.1021/acscatal.6b02726
ACS Catal. 2016, 6, 8350−8360

of the coumarin−OH adduct (7-hydroxycoumarin (7-HC)), which is generated via the reaction of coumarin with a hydroxyl radical.[45] Figure 7a shows the time profiles of 7-HC generation

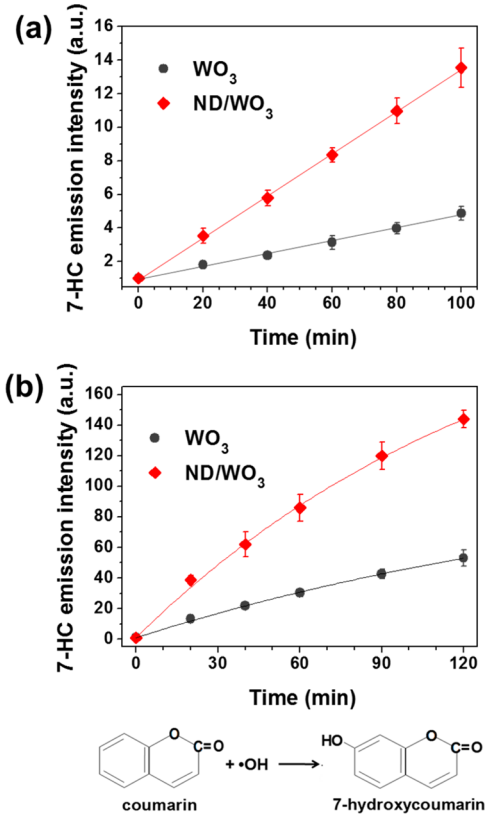

Figure 7. Time profiles of the coumarin−OH adduct (7-hydroxycoumarin: 7-HC) production in the suspension of bare WO_3 and ND(8 wt %)/WO_3 under visible-light illumination (λ > 420 nm) in the (a) absence and (b) presence of 5 mM H_2O_2 ([catalyst] = 1 g L^{-1}, $[coumarin]_0$ = 6.8 mM, pH_i 2.0). The relative concentration of 7-HC was measured by monitoring the emission intensity at 455 nm.

in the aqueous suspension of bare WO_3 and ND(8 wt %)/WO_3 under visible-light illumination (λ > 420 nm). ND/WO_3 showed much higher production of 7-HC than bare WO_3, which implies that the production of OH radicals is favored on ND/WO_3. This is consistent with the higher photocatalytic activity of ND/WO_3 for the degradation of acetaldehyde. The OH radicals can be generated via two pathways: one from the hole oxidative path,

$$H_2O + h^+ \rightarrow \bullet OH + H^+$$

and the other from the O_2 reduction path,

$$O_2 + 2H^+ + 2e^- \rightarrow H_2O_2$$

$$H_2O_2 + H^+ + e^- \rightarrow H_2O + \bullet OH$$

To test which pathway is more dominant, we further evaluated the production of 7-HC in the presence of H_2O_2 under visible-light illumination (λ > 420 nm) (see Figure 7b). The 7-HC production rate was significantly increased in the presence of H_2O_2, which supports the belief that the OH radical is generated mainly through the reductive pathway. Since H_2O_2 can scavenge holes,

$$H_2O_2 + h^+ \rightarrow HO_2^\bullet + H^+$$

its presence should suppress the OH radical generation through the oxidative pathway. In addition, if 7-HC had been generated from the reaction of coumarin with the hole (not OH radical), the generation of 7-HC would have been hindered in the presence of H_2O_2.

These photoelectrochemical and photochemical results collectively confirm that ND on WO_3 effectively retards the charge recombination through the interfacial electron transfer from WO_3 CB to the surface conducting layer on ND and reduces the overpotential of O_2 reduction. The effect of ND can be similarly compared with the role of platinum loaded on WO_3 in many ways. The production of OH radicals is enabled through the utilization of O_2 as a CB electron scavenger via multielectron transfer[13,19] and the fast decomposition of H_2O_2 into OH radicals.

Photocatalytic Stability of ND/WO_3. The stability of ND/WO_3 was tested for the photocatalytic decomposition of acetaldehyde with repeated cycles, as shown in Figure 8. After

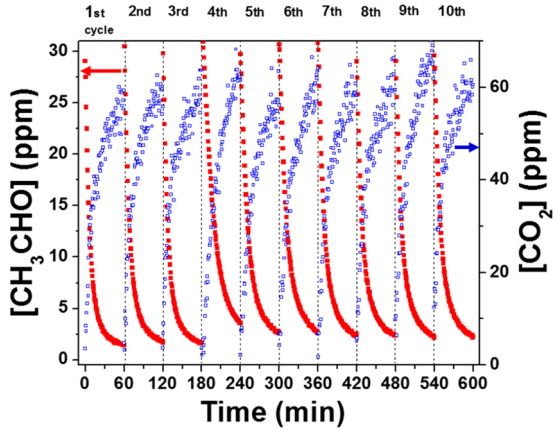

Figure 8. Repeated runs for the photocatalytic degradation of acetaldehyde (CH_3CHO) and the concurrent production of carbon dioxide (CO_2) on ND(8 wt %)/WO_3 under visible-light illumination (λ > 420 nm), $[CH_3CHO]_0$ = 30 ppmv.

performing the photocatalytic reaction for 1 h when most of acetaldehyde was decomposed, the same amount of acetaldehyde was added again into the reactor and the subsequent photocatalysis cycle was restarted. Note that both acetaldehyde decomposition and CO_2 production on the visible-light-irradiated ND/WO_3 exhibited little change during the repeated photocatalysis runs up to 10 cycles, confirming the stability of the hybrid photocatalyst.

CONCLUSIONS

The combination of a base semiconductor with a noble-metal co-catalyst is a common strategy for the development of efficient photocatalyst. In this study, we employed nanodiamonds (NDs) that consist of Earth-abundant elemental carbon only as a co-catalyst to replace expensive noble metals, prepared ND-loaded WO_3 as an effective visible-light-driven photocatalyst, and demonstrated its highly enhanced activity, compared with bare WO_3 for the degradation of volatile organic compounds (VOCs) under visible light. Such superior activity of ND/WO_3 (comparable to Pt/WO_3) is attributed to the enhanced charge separation, interfacial electron transfer, and lower overpotential of O_2 reduction, which is enabled by the role of NDs that is similarly compared with the Pt co-catalyst that utilizes O_2 as a conduction band (CB) electron scavenger

DOI: 10.1021/acscatal.6b02726
ACS Catal. 2016, 6, 8350−8360

via multielectron transfer. We found that the presence of a graphitic carbon shell (sp^2) on the diamond core (sp^3) plays a vital role for charge separation and the subsequent interfacial electron transfer. The photocatalytic activity of ND-loaded WO_3 was sensitively influenced by removing/increasing the graphitic layer and modifying the surface functional groups. The use of NDs as Earth-abundant carbon nanomaterials is proposed as a cost-effective method to replace expensive noble-metal co-catalysts (i.e., Pt, Pd) for photocatalytic air purification.

■ ASSOCIATED CONTENT

Supporting Information

The Supporting Information is available free of charge on the ACS Publications website at DOI: 10.1021/acscatal.6b02726.

Additional table and analysis data of zeta (ζ) potential, XPS, FE-SEM, XRD, FT-IR, UV/visible absorption spectra, HR-TEM images, EDS, and photocatalytic acitivity tests (PDF)

■ AUTHOR INFORMATION

Corresponding Author

*Tel.: +82-54-279-2283. Fax: +82-54-279-8299. E-mail: wchoi@postech.edu.

ORCID

Wonyong Choi: 0000-0003-1801-9386

Author Contributions

§These authors contributed equally to this work.

Notes

The authors declare no competing financial interest.

■ ACKNOWLEDGMENTS

This research was financially supported by the Global Research Laboratory (GRL) Program (No. NRF-2014K1A1A2041044) and KCAP (Sogang Univ.) (No. 2009-0093880), which were funded by the Korea Government (MSIP) through the National Research Foundation (NRF).

■ REFERENCES

(1) Hoffmann, M. R.; Martin, S. T.; Choi, W. Y.; Bahnemann, D. W. *Chem. Rev.* **1995**, *95*, 69−96.
(2) Park, H.; Park, Y.; Kim, W.; Choi, W. *J. Photochem. Photobiol., C* **2013**, *15*, 1−20.
(3) Park, H.; Kim, H. I.; Moon, G. H.; Choi, W. *Energy Environ. Sci.* **2016**, *9*, 411−433.
(4) Friedmann, D.; Mendive, C.; Bahnemann, D. *Appl. Catal., B* **2010**, *99*, 398−406.
(5) Kim, H.; Choi, W. *Appl. Catal., B* **2007**, *69*, 127−132.
(6) Robert, D. *Catal. Today* **2007**, *122*, 20−26.
(7) Sheng, H.; Ji, H. W.; Ma, W. H.; Chen, C. C.; Zhao, J. C. *Angew. Chem., Int. Ed.* **2013**, *52*, 9686−9690.
(8) Strukul, G. *Catalytic Oxidations with Hydrogen Peroxide as Oxidant*, Vol. *9*; Kluwer Academic Publishers: Dordrecht, The Netherlands, 1992; p 101.
(9) Arai, T.; Yanagida, M.; Konishi, Y.; Iwasaki, Y.; Sugihara, H.; Sayama, K. *J. Phys. Chem. C* **2007**, *111*, 7574−7577.
(10) Irie, H.; Miura, S.; Kamiya, K.; Hashimoto, K. *Chem. Phys. Lett.* **2008**, *457*, 202−205.
(11) Arai, T.; Horiguchi, M.; Yanagida, M.; Gunji, T.; Sugihara, H.; Sayama, K. *Chem. Commun.* **2008**, 5565−5567.
(12) Arai, T.; Yanagida, M.; Konishi, Y.; Iwasaki, Y.; Sugihara, H.; Sayama, K. *Catal. Commun.* **2008**, *9*, 1254−1258.
(13) Abe, R.; Takami, H.; Murakami, N.; Ohtani, B. *J. Am. Chem. Soc.* **2008**, *130*, 7780−7781.
(14) Xiang, Q.; Meng, G. F.; Zhao, H. B.; Zhang, Y.; Li, H.; Ma, W. J.; Xu, J. Q. *J. Phys. Chem. C* **2010**, *114*, 2049−2055.
(15) Sun, S. M.; Wang, W. Z.; Zeng, S. Z.; Shang, M.; Zhang, L. *J. Hazard. Mater.* **2010**, *178*, 427−433.
(16) Liu, Z. F.; Zhao, Z. G.; Miyauchi, M. *J. Phys. Chem. C* **2009**, *113*, 17132−17137.
(17) Yeager, E. *Electrochim. Acta* **1984**, *29*, 1527−1537.
(18) Wang, Y. X.; Balbuena, P. B. *J. Phys. Chem. B* **2005**, *109*, 14896−14907.
(19) Kim, J.; Lee, C. W.; Choi, W. *Environ. Sci. Technol.* **2010**, *44*, 6849−6854.
(20) Danilenko, V. V. *Phys. Solid State* **2004**, *46*, 595−599.
(21) Maze, J. R.; Stanwix, P. L.; Hodges, J. S.; Hong, S.; Taylor, J. M.; Cappellaro, P.; Jiang, L.; Dutt, M. V. G.; Togan, E.; Zibrov, A. S.; Yacoby, A.; Walsworth, R. L.; Lukin, M. D. *Nature* **2008**, *455*, 644−641.
(22) Chang, Y. R.; Lee, H. Y.; Chen, K.; Chang, C. C.; Tsai, D. S.; Fu, C. C.; Lim, T. S.; Tzeng, Y. K.; Fang, C. Y.; Han, C. C.; Chang, H. C.; Fann, W. *Nat. Nanotechnol.* **2008**, *3*, 284−288.
(23) Huang, H.; Pierstorff, E.; Osawa, E.; Ho, D. *Nano Lett.* **2007**, *7*, 3305−3314.
(24) Jang, D. M.; Myung, Y.; Im, H. S.; Seo, Y. S.; Cho, Y. J.; Lee, C. W.; Park, J.; Jee, A. Y.; Lee, M. *Chem. Commun.* **2012**, *48*, 696−698.
(25) Gaillard, C.; Girard, H. A.; Falck, C.; Paget, V.; Simic, V.; Ugolin, N.; Bergonzo, P.; Chevillard, S.; Arnault, J. C. *RSC Adv.* **2014**, *4*, 3566−3572.
(26) Hu, Y.; Jensen, J. O.; Zhang, W.; Martin, S.; Chenitz, R.; Pan, C.; Xing, W.; Bjerrum, N. J.; Li, Q. F. *J. Mater. Chem. A* **2015**, *3*, 1752−1760.
(27) Shenderova, O. A.; McGuire, G. Nanocrystalline Diamond. In *Nanomaterials Handbook*; Gogotsi, Y., Ed.; CRC Taylor and Francis Group: Boca Raton, FL, 2006; pp 203−237.
(28) Mochalin, V. N.; Shenderova, O.; Ho, D.; Gogotsi, Y. *Nat. Nanotechnol.* **2011**, *7*, 11−23.
(29) Pastrana-Martinez, L. M.; Morales-Torres, S.; Carabineiro, S. A. C.; Buijnsters, J. G.; Faria, J. L.; Figueiredo, J. L.; Silva, A. M. T. *ChemPlusChem* **2013**, *78*, 801−807.
(30) Kim, K. D.; Dey, N. K.; Seo, H. O.; Kim, Y. D.; Lim, D. C.; Lee, M. *Appl. Catal., A* **2011**, *408*, 148−155.
(31) Sampaio, M. J.; Pastrana-Martínez, L. M.; Silva, A. a. M. T.; Buijnsters, J. G.; Han, C.; Silva, C. a. G.; Carabineiro, S. o. A. C.; Dionysiou, D. D.; Faria, J. L. *RSC Adv.* **2015**, *5*, 58363−58370.
(32) Osswald, S.; Yushin, G.; Mochalin, V.; Kucheyev, S. O.; Gogotsi, Y. *J. Am. Chem. Soc.* **2006**, *128*, 11635−11642.
(33) Cebik, J.; McDonough, J. K.; Peerally, F.; Medrano, R.; Neitzel, I.; Gogotsi, Y.; Osswald, S. *Nanotechnology* **2013**, *24*, 205703.
(34) Kim, H.-i.; Moon, G.; Monllor-Satoca, D.; Park, Y.; Choi, W. *J. Phys. Chem. C* **2012**, *116*, 1535−1543.
(35) Marcano, D. C.; Kosynkin, D. V.; Berlin, J. M.; Sinitskii, A.; Sun, Z. Z.; Slesarev, A.; Alemany, L. B.; Lu, W.; Tour, J. M. *ACS Nano* **2010**, *4*, 4806−4814.
(36) Zhang, H.; Lv, X.; Li, Y.; Wang, Y.; Li, J. *ACS Nano* **2010**, *4*, 380−386.
(37) Ma, S. S. K.; Hisatomi, T.; Maeda, K.; Moriya, Y.; Domen, K. *J. Am. Chem. Soc.* **2012**, *134*, 19993−19996.
(38) Fang, J.; Wang, F.; Qian, K.; Bao, H. Z.; Jiang, Z. Q.; Huang, W. X. *J. Phys. Chem. C* **2008**, *112*, 18150−18156.
(39) Yun, H. J.; Lee, H.; Joo, J. B.; Kim, N. D.; Kang, M. Y.; Yi, J. *Appl. Catal., B* **2010**, *94*, 241−247.
(40) Park, Y.; Singh, N. J.; Kim, K. S.; Tachikawa, T.; Majima, T.; Choi, W. *Chem.—Eur. J.* **2009**, *15*, 10843−10850.
(41) Kim, H.-i.; Kim, J.; Kim, W.; Choi, W. *J. Phys. Chem. C* **2011**, *115*, 9797−9805.
(42) Park, H.; Choi, W. *J. Phys. Chem. B* **2004**, *108*, 4086−4093.
(43) Shin, H.; Kim, H. I.; Chung, D. Y.; Yoo, J. M.; Weon, S.; Choi, W.; Sung, Y. E. *ACS Catal.* **2016**, *6*, 3914−3920.

DOI: 10.1021/acscatal.6b02726
ACS Catal. 2016, 6, 8350−8360

(44) Bader, H.; Sturzenegger, V.; Hoigne, J. *Water Res.* **1988**, *22*, 1109−1115.
(45) Ishibashi, K.; Fujishima, A.; Watanabe, T.; Hashimoto, K. *Electrochem. Commun.* **2000**, *2*, 207−210.
(46) Lin, Y. M.; Su, D. S. *ACS Nano* **2014**, *8*, 7823−7833.
(47) Yang, L.; May, P. W.; Yin, L.; Smith, J. A.; Rosser, K. N. *Diamond Relat. Mater.* **2007**, *16*, 725−729.
(48) Moon, G. H.; Kim, W.; Bokare, A. D.; Sung, N. E.; Choi, W. *Energy Environ. Sci.* **2014**, *7*, 4023−4028.
(49) Ong, T. P.; Chang, R. P. H. *Appl. Phys. Lett.* **1989**, *55*, 2063−2065.
(50) Saslow, W.; Bergstresser, T. K.; Cohen, M. L. *Phys. Rev. Lett.* **1966**, *16*, 354−356.
(51) Wang, W. D.; Serp, P.; Kalck, P.; Faria, J. L. *J. Mol. Catal. A: Chem.* **2005**, *235*, 194−199.
(52) Zhang, Y. H.; Tang, Z. R.; Fu, X.; Xu, Y. J. *ACS Nano* **2011**, *5*, 7426−7435.
(53) Kim, H.-i.; Moon, G. H.; Monllor-Satoca, D.; Park, Y.; Choi, W. *J. Phys. Chem. C* **2012**, *116*, 1535−1543.
(54) Weon, S.; Choi, W. *Environ. Sci. Technol.* **2016**, *50*, 2556−2563.
(55) Kim, H.-i.; Kwon, O. S.; Kim, S.; Choi, W.; Kim, J. H. *Energy Environ. Sci.* **2016**, *9*, 1063−1073.
(56) Chakrapani, V.; Angus, J. C.; Anderson, A. B.; Wolter, S. D.; Stoner, B. R.; Sumanasekera, G. U. *Science* **2007**, *318*, 1424−1430.
(57) Nebel, C. E. *Science* **2007**, *318*, 1391−1392.
(58) Moon, G. H.; Kim, D. H.; Kim, H.-i.; Bokare, A. D.; Choi, W. *Environ. Sci. Technol. Lett.* **2014**, *1*, 185−190.
(59) Jiang, T.; Xu, K. *Carbon* **1995**, *33*, 1663−1671.
(60) Jiang, T. L.; Xu, K.; Ji, S. F. *J. Chem. Soc., Faraday Trans.* **1996**, *92*, 3401−3406.
(61) Yushin, G. N.; Osswald, S.; Padalko, V. I.; Bogatyreva, G. P.; Gogotsi, Y. *Diamond Relat. Mater.* **2005**, *14*, 1721−1729.
(62) Prawer, S.; Nugent, K. W.; Jamieson, D. N.; Orwa, J. O.; Bursill, L. A.; Peng, J. L. *Chem. Phys. Lett.* **2000**, *332*, 93−97.
(63) Ferrari, A. C.; Robertson, J. *Philos. Trans. R. Soc., A* **2004**, *362*, 2477−2512.
(64) Mermoux, M.; Crisci, A.; Petit, T.; Girard, H. A.; Arnault, J. C. *J. Phys. Chem. C* **2014**, *118*, 23415−23425.
(65) Park, Y.; Kang, S. H.; Choi, W. *Phys. Chem. Chem. Phys.* **2011**, *13*, 9425−9431.
(66) Amanullah, S.; Das, P. K.; Samanta, S.; Dey, A. *Chem. Commun.* **2015**, *51*, 10010−10013.

DOI: 10.1021/acscatal.6b02726
ACS Catal. 2016, 6, 8350−8360